Proc. Indian Acad. Sci. (*Chem. Sci.*), Vol. 113, Nos 5 & 6, October–December 2001, pp 393–413

Relaxation in binary mixtures: Non-ideality, heterogeneity and re-entrance

ARNAB MUKHERJEE, GOUNDLA SRINIVAS,
SARIKA BHATTACHARYYA and BIMAN BAGCHI*
Solid State and Structural Chemistry Unit, Indian Institute of Science,
Bangalore 560 012, India
e-mail: bbagchi@sscu.iisc.ernet.in

Abstract. Binary mixtures show many kinds of fascinating dynamical behaviour which has eluded microscopic description till very recently. In this work we show that much of the anomalous behaviour can be explained by building suitable models and carrying out theoretical and simulation studies. Specifically, three well-known problems have been addressed here. (a) Non-ideality in composition dependence of viscosity, (b) re-entrant behaviour of orientational relaxation, and (c) heterogeneity in supercooled binary mixtures. The physical origin of the dynamical behaviour of binary mixtures can be understood in terms of composition fluctuation, a study of which has also been presented in this paper.

Keywords. Binary mixtures; non-ideality; orientational relaxation; composition fluctuation.

1. Introduction

Binary mixtures are ubiquitous in chemistry. Most chemical solvents are multi-component and in particular binary. In a binary mixture, by altering the composition of one of the ingredients one can change solubility, polarisability, viscosity and many other static and dynamic properties. This tunability is of great use in chemistry. Although the static and dynamic properties of many mixtures are well characterized, a general theoretical framework to understand dynamic properties particularly is still lacking.

The elegant theory of Kirkwood and Buff can be used to explain many aspects of static properties[1] but the same is not available for the dynamical properties. This is somewhat surprising, given the fact that the dynamic properties in a binary mixture show exotic features which pose interesting challenges to theoreticians. Among them the extrema observed in the composition dependence of excess viscosity[2,3], the anomalous viscosity dependence of the rotational relaxation time[4] and the heterogeneous dynamics near glass transition are certainly the most important ones. Highly non-exponential solvation dynamics has been observed in binary dipolar mixtures[5–7]. In recent years, a large number of studies have been devoted to glass transition and glassy behaviour in binary mixture on Kob–Andersen model[8,9] but with a single composition $x_A = 0{\cdot}8$ and $x_B = 0{\cdot}2$[10,11]. None of these studies has addressed the well-known anomalous composition dependence.

*For correspondence

In a binary mixture, there is a choice of three different interactions, two length scales and two different masses. A combination of all these different parameters gives rise to several microscopic time scales in the system. Thus the equilibrium and dynamic properties in these systems are considerably different from that of an one component system. In addition to the multiple time scales, binary mixtures have interesting relaxational dynamics which are controlled not only by density and momenta relaxation but also by the composition fluctuation, which plays an important role. This is particularly true when interaction energies between the two constituents and also the sizes differ significantly. If the free energy cost of composition fluctuation is not very large then it becomes a convenient channel for stress and other relaxation. The composition fluctuation can also be rather slow as it involves exchange of atoms. Given the diversity present in the system it is naive to expect any simple theory to explain the anomalies present in a binary mixture. In fact, very little understanding of a binary mixture is possible by studying a one-component system.

In this article we will address the above mentioned anomalies present in the binary mixture. In addition to this we will also present a study of the probability of composition fluctuation in a binary mixture. To capture the various aspects of composition dependence of viscosity, we have introduced two new models (subsequently called model I and model II). Model I is of attractive or structure-making kind owing to the very strong interaction between two different components of the binary mixture whereas model II is of repulsive or structure-breaking kind as the different components have very little interaction between themselves. We carried out mode coupling theory (MCT) calculation and NVE (constant number N, volume V and energy E) and NPT (constant number N, pressure P and temperature T) simulation on the two above models to show that even the two very simple models above can contain the anomalous composition dependence of viscosity. The composition fluctuation is studied from NVE molecular dynamics simulation results. NPT molecular dynamics simulation of Gay–Berne ellipsoids in a Lennard–Jones binary mixture is performed to study the anomalous viscosity dependence of the orientational relaxation [12]. We showed that the orientational relaxation time has a re-entrant viscosity dependence for different composition which indicates in a dramatic fashion that viscosity is not an unique determinant of relaxation time. A similar system of Gay–Berne ellipsoids in a binary Lennard-Jones mixture is used to study the heterogeneous orientational dynamics [13]. The parameters in the binary system in this study are the same as Kob–Andersen model. In this system at high pressure the orientational relaxation dynamics is indeed heterogeneous.

Organization of the rest of the paper is as follows. In §2, we address the non-ideality in the composition dependence of viscosity in a binary mixture and also show the correlation between excess volume and excess viscosity. In §3, the probability distribution for composition fluctuation is presented. In §4, anomalous viscosity dependence of orientational correlation is discussed. Section 5 is devoted to the study of heterogeneous dynamics in orientational relaxation in supercooled liquids. The article is concluded with a brief discussion in §6.

2. Non-ideal composition dependence of viscosity: Correlation between excess viscosity and excess volume

It is generally believed that the total viscosity increases on mixing if the two different components of a binary mixture attract each other and decreases when the different

ingredients of the mixture repel each other. In a real mixture, an observed property P is often very different from its predicted ideal value P_{id} given by [14],

$$P_{id} = x_A P_A + x_B P_B, \tag{1}$$

where x_A and x_B are the mole fractions and P_A and P_B are the values of the property P of the corresponding pure (single component) liquids. Now we define the corresponding excess quantity P_{excess} as,

$$P_{excess} = P - P_{id}. \tag{2}$$

These quantities, i.e. P and P_{excess} can be any dynamic or static quantities such as viscosity (η), specific heat, volume etc. Departure from (1) is attributed to the specific interaction between the two components of the mixture. While the reason for this deviation is often discussed in terms of the above mentioned attraction or repulsion between the constituents, quantitative understanding of these phenomena from microscopic theory has remained largely incomplete. In order to address this problem, we constructed two different binary mixture models (referred to as model I and model II) in which the strength of the solute–solvent interaction is varied by keeping *all the other parameters* unchanged. All the three interactions are described by either the Lennard–Jones or the modified Lennard–Jones potential. In model I, specific structure formation between solute and solvent molecules is mimicked by stronger solute–solvent attractive interaction ($\varepsilon_{AB} = 2{\cdot}0$) than that between solvent–solvent ($\varepsilon_{AA} = 1{\cdot}0$) and solute–solute ($\varepsilon_{BB} = 0{\cdot}5$) interactions. The second model (model II) involves structure-breaking by weak solute–solvent interaction ($\varepsilon_{AB} = 0{\cdot}3$). These two models are perhaps the simplest models to mimic structure-making and structure-breaking in binary mixtures. For convenience, we denote the solvent molecules as A, and the solute molecules as B. In both the models, A and B have the same radii and the same masses. In this section, we carry out both MCT calculation and extensive NVE and NPT molecular dynamics simulations to evaluate the non-ideality in the composition dependence of viscosity and we have also established the correlation between excess volume (Vol_{excess}) and excess viscosity (η_{excess}) throughout the composition range for both the models. Note that the latter part needs the simulation to be carried out through the NPT ensemble method as NVE simulation does not allow volume fluctuation.

2.1 *Basic definitions*

In this subsection, we describe the outlines of basic microscopic expressions of viscosity. This also gives us the opportunity to explain the expressions that appear in the theoretical formulation in this section later. The microscopic expression for the time-dependent shear viscosity is formulated in terms of stress autocorrelation function and is given by [15,16],

$$\eta(t) = (1/Vk_BT)\,\langle \sigma^{xz}(0)\,\sigma^{xz}(t)\rangle, \tag{3}$$

where σ^{xz} is the off-diagonal element of the stress tensor given by,

$$\sigma^{xz} = \sum_{j=1}^{N}[(p_j^x p_j^z/m) + F_j^z x_j]. \tag{4}$$

Here F_j^z is the z-component of the force acting on the jth particle and the corresponding position of the jth particle is x_j, p_j^z is the z-component of the momentum of the jth particle, m being the mass of the particle. N is the total number of particles which is also equal to $N_A + N_B$. Here N_A is the number of solvent particles and N_B is the number of solute particles present in the mixture. High frequency shear modulus, known as G_∞, is equal to the zero-time stress autocorrelation function [15,16],

$$G_\infty = (1/Vk_BT) \langle (\sigma^{xz}(0))^2 \rangle, \tag{5}$$

and finally the frequency dependent viscosity is obtained by Laplace transforming $\eta(t)$,

$$\eta(z) = \int_0^\infty \mathrm{d}t \exp(-zt)\eta(t). \tag{6}$$

Experimentally observed viscosity is given by the zero frequency limit of $\eta(z)$.

2.2 *Formulation of the mode coupling theory*

Any formulation of the mode coupling theory (MCT) starts by separating the fast short-time decay from the slow long-time decay of the relevant time correlation function (TCF). The short-time decay is assumed to occur from a few body (mainly binary) interactions whereas the long-time decay is assumed to occur from coupling of the TCF to the binary product of the slow collective modes. Thus the expression for the viscosity can be decomposed into two parts and written as [18,19]

$$\eta(t) = \eta_{\text{short}}(t) + \eta_{\text{collective}}(t). \tag{7}$$

Thus, central to the mode coupling theory development of any time correlation function is this assumption of the separation of time scales between the fast initial decay and the slow long-time decay. The robustness of a mode coupling theory calculation actually depends critically on the accurate evaluation of the short time part [17]. Not only does the short time part (often called the 'bare' term) often contribute about 50% to the value of the transport coefficient (here viscosity), but also determines the magnitude of the contribution of the long-time part. In fact, a central ingredient of both the short- and the long-time contributions is the static correlation functions. The short-time contribution, often referred to as the binary term, is assumed to be given by a Gaussian approximation. The rational for this assumption comes from the observation that only the even powers of time (t) appear in the short-time expansion of $\eta(t)$ and collective term contribution starts as t^4. So the t^2 term contribution to binary viscosity can be approximated as a Gaussian function and can be written as [18–20],

$$\eta^{\text{bin}}(t) = G_\infty \exp(-t^2/\tau_\eta^2), \tag{8}$$

where τ_η, appearing in the above expression, can be determined by the second derivative of $\eta(t)$. For pure liquids, calculations of binary terms have been reported by Balucani [21] and also by Bhattacharyya and Bagchi [17,22]. The expression of the infinite frequency shear modulus, G_∞, is given with the help of (4) and (5),

$$G_\infty = (\rho_1 + \rho_2)k_BT + \frac{2\pi}{15}\sum_{i,j=1}^{2}\rho_i\rho_j\int_0^\infty \mathrm{d}r g_{ij}(r)\frac{\mathrm{d}}{\mathrm{d}r}\left[r^4\frac{\mathrm{d}v_{ij}(r)}{\mathrm{d}r}\right], \tag{9}$$

where, $i, j = 1$ indicate (A) particles and $i, j = 2$ denote (B) particles. Thus, ρ_1 is the number density for the solvent particles and ρ_2 denotes the same for the solute particles. $g_{ij}(r)$ is the partial radial distribution function of the particles labeled i and j. Note that v_{ij} includes three different interaction potentials present between the solute and the solvent particles. By using (8), the expression for τ_h can be written as,

$$\tau_h = \left(\frac{-2G_\infty}{\dot{\eta}_{\mathrm{mix}}(t=0)}\right)^{1/2}. \tag{10}$$

Expression of $\dot{\eta}_{\mathrm{mix}}(t=0)$ is complicated and given elsewhere [23].

The collective or mode coupling contribution to viscosity has been evaluated by Bosse *et al*[24] and further developed by Geszti [25]. In this approach one starts with the general time correlation function expression for the shear viscosity in terms of the transverse current. One starts with a Mori-type rephrasing of the Green–Kubo formula for the shear viscosity. Thus the expression for the viscosity can be written as,

$$\eta = \lim_{\epsilon\to 0}\lim_{q\to 0}\frac{m^2}{q^2V}\int_0^\infty \mathrm{d}t(QLj^x(\mathbf{q}) \mid \exp(iQLQT - \epsilon t) \mid QLj^x(\mathbf{q})). \tag{11}$$

In the above equation, **q** has been considered to be aligned along the z direction. L is the Hermitian–Liouville operator, $Q = 1–P$, where P is the projection operator which projects on to the chosen dynamical variable A^a. A^a is the set of slow variables which consists of three current densities and two particle densities for both the components which constitute the binary mixture. After a few steps of calculation, the MCT expression of viscosity takes the form below [23],

$$\eta_{\rho_i\rho_j} = \frac{k_BT}{60\pi^2}\int_0^\infty \mathrm{d}q\, q^4\frac{S'_{ii}(q)S'_{jj}(q)}{S^2_{ii}(q)S^2_{jj}(q)}\int_{\tau_h}^\infty \mathrm{d}t F^2_{ij}(q,t), \tag{12}$$

where, $S_{ii}(q)$ is the static structure factor and $S'_{ii}(q) = \frac{\partial}{\partial q}S_{ii}(q)$. $S'_{ii}(q)$ has been obtained using soft mean spherical approximation (SMSA) closure [26]. $F_{ij}(q, t)$ is the dynamic input parameter and in this case the different $F_{ij}(q, t)$ are calculated from time-dependent density functional theory [27]. Note that the lower limit of the time integration has been changed from zero to τ_h to take out all the contributions of the order t^2 as the collective contributions are expected to start as t^4. τ_h is the characteristic time for Gaussian decay that appeared in the expression of binary viscosity in (8). The total mode coupling contribution to the viscosity is obtained by summing together all the $\eta_{\rho_i\rho_j}$ terms,

$$\eta_{rr} = \sum_{i,j=1}^{2} \eta_{r_i r_j}. \tag{13}$$

2.3 *Simulation details*

We have carried out a series of both NVE and NPT simulations[23,28,29] of binary mixtures by varying the solute mole fraction from 0 to 1. Our model binary systems consist of a total of 500 (solvent (A) + solute (B)) particles. In case of NVE simulation, we used the Lennard–Jones 12-6 potential,

$$U_{ij} = 4\varepsilon_{ij}[(\sigma / r_{ij})^{12} - (\sigma / r_{ij})^{6}], \tag{14}$$

whereas in case of NPT simulation, interaction between any two particles is given by the modified Lennard–Jones potential which sets a cutoff radius r_c, outside which the potential energy is zero. The particular form of the potential is given by [30],

$$U_{ij} = 4\varepsilon_{ij}\left\{\left[\left(\frac{\sigma}{r_{ij}}\right)^{12} - \left(\frac{\sigma}{r_{ij}}\right)^{6}\right] + \left[6\left(\frac{\sigma}{r_c}\right)^{12} - 3\left(\frac{\sigma}{r_c}\right)^{6}\right]\left(\frac{r}{r_c}\right)^{2} - 7\left(\frac{\sigma}{r_c}\right)^{12} + 4\left(\frac{\sigma}{r_c}\right)^{6}\right\}, \tag{15}$$

where the cutoff distance r_c in this particular case has been taken as equal to $2{\cdot}5\sigma$. Use of the above potential form takes care of the fact that both potential and force are continuous at the cutoff distance. *i* and *j* in (14) and (15) denote two different particles. We set the diameter (σ) and mass (m) of both the solute and the solvent to unity, for simplicity. The solute–solvent interaction strength lies in the potential well depth ε_{AB}, where A and B represent the solvent and solute particles respectively. Throughout this study we keep the interaction strength $\varepsilon_{AA} = 1{\cdot}0\varepsilon$, (solvent–solvent), $\varepsilon_{BB} = 0{\cdot}5\varepsilon$ (solute–solute). We dealt with two very different specific solvent–solute interaction strength values, referred as model I and model II. In model I, $\varepsilon_{AB} = 2{\cdot}0\varepsilon$ and in model II, $\varepsilon_{AB} = 0{\cdot}3\varepsilon$. While the former accounts for the situation in which the solute and solvent particles attract each other more strongly than they do amongst themselves, the latter describes the opposite scenario. Henceforth we will be referring to the situations in which $\varepsilon_{AB} = 2{\cdot}0$ and $\varepsilon_{AB} = 0{\cdot}3$ the *attractive* and *repulsive* respectively. We set the reduced temperature T^* ($= k_BT/\varepsilon$) as 1·0 in model I and 1·24 in model II. After many trial runs to verify the existing results on viscosity [31] of one-component liquids, we selected a time step $\Delta t^* = 0{\cdot}002\tau$ for model I and $\Delta t^* = 0{\cdot}001\tau$ for model II for the integration of the Newtonian equations of motion. The scaled time has been denoted as $\tau = \sigma(m/\varepsilon)^{1/2}$. We have dealt with eight different solute compositions, namely 0·0, 0·1, 0·2, 0·4, 0·6, 0·8, 0·9 and 1·0. For each solute composition we have equilibrated the system up to $1{\cdot}5 \times 10^5$ time steps. Simulations have been carried out for another 2×10^5 production steps after equilibration in NVE simulation and 10^6 production steps in case of NPT simulation, during which the stress tensor has been calculated. In case of NPT simulation, pressure is kept constant at 2·0 (ε/σ^3) by Anderson's piston method [32], while in the case of temperature, a damped oscillator method has been adopted which keeps temperature constant at each and every step [33]. We have done *three* different simulation

runs for each composition point where each of the last two runs has been started from the particle positions and velocities stored in the last time step of the previous simulation. We have also calculated the radial distribution function in each case to make sure that the clustering or phase separation (especially among similar species) is avoided.

2.4 Results and discussion

Figure 1 depicts the non-ideality of viscosity obtained from both NVE simulation and mode coupling theory with respect to solute (B) composition, for both the models. Though the agreement between theory and simulation is certainly not perfect, the trends are similar in both the calculations. Note that the theoretical calculation does not use *any simulation data* as input or *any adjustable parameter* either; thus theory and simulation provide tests independent of each other which is important for binary mixtures.

Figures 2 and 3 show the correlation between excess volume and excess viscosity given by (2). The results of these figures are drawn out from NPT simulation as NVE simulation does not allow volume change.

Figure 2a shows the positive deviation of viscosity and figure 2b the negative deviation of volume, from their ideal values for model I. Figure 3a, on the other hand, shows negative deviation of viscosity and figure 3b the positive deviation of volume for model II. Note that the correlation between excess volume and excess viscosity is always opposite and in the two different models they manifest in opposite ways. The results presented in figures 1–3 can be partly understood by analysing the microscopic structure. In figures 4a and b we plot all the partial radial distribution function ($g_{AA}(r)$, $g_{BB}(r)$ and $g_{AB}(r)$) obtained from the NPT simulation, for models I and II respectively. As the solute–solvent interaction strength affects the structure surrounding a

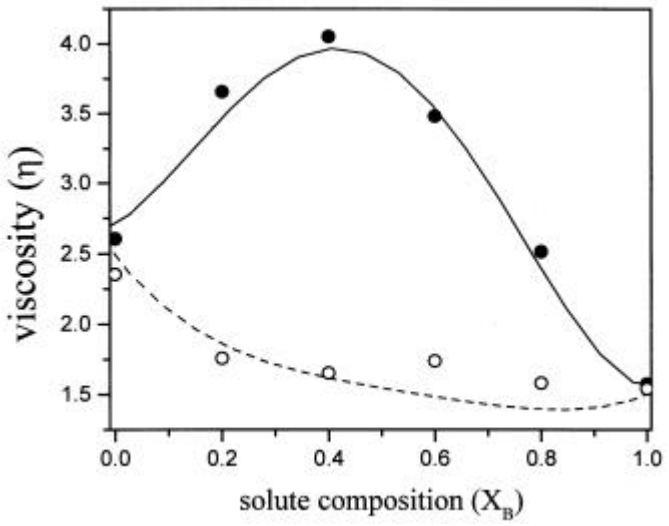

Figure 1. The composition dependence of viscosity obtained from NVE MD simulations (symbols) and mode coupling theory (lines) for both the models. Filled (open) circles show simulation results for model I (model II). The lines show the theories.

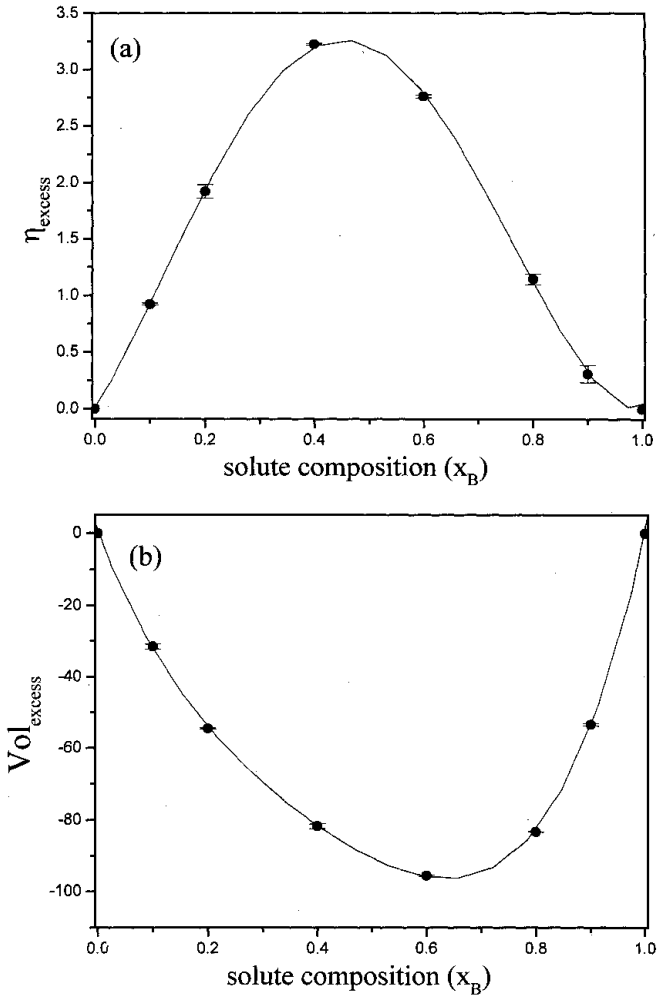

Figure 2. Composition dependence of excess viscosity and excess volume for model I. In (**a**), the calculated excess viscosity (h_{excess}) is plotted against solute composition (x_B) for model I. In (**b**), the variation of excess volume (Vol_{excess}) with solute composition (x_B) is plotted for the same model. Solid lines are just for guidance to the eye.

solute/solvent to a great extent[34–36], the above observed features are reflected in the *increment of correlation among the unlike species*, $g_{AB}(r)$, in figure 4a for model I while the reverse is seen in figure 4b for model II. We can refer to such behaviour as "structure-forming" in model I and "structure-breaking" in model II.

The above figures can explain the complex phenomena of non-ideality in dynamic properties from very simple microscopic models which explain that the key to the non-ideality of mixtures belongs to the nature of interaction between the different species constituting the mixture.

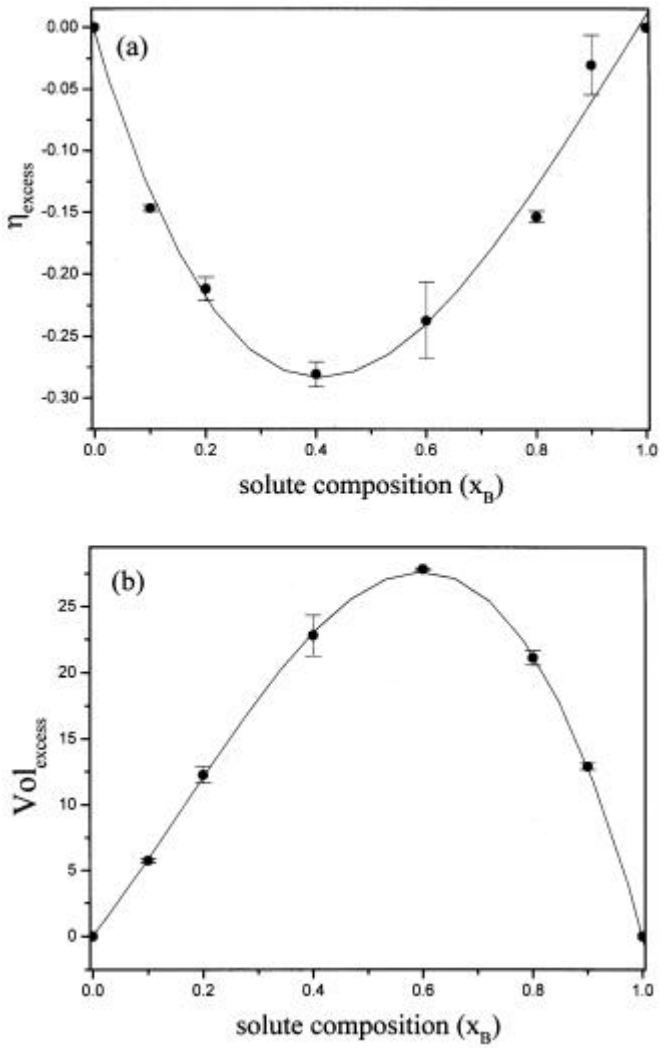

Figure 3. Composition dependence of excess viscosity and excess volume for model II. In (**a**), the excess viscosity (h_{excess}) is plotted against solute composition (x_B) for model II. In (**b**), excess volume (Vol_{excess}) is plotted against the solute coposition (x_B) for model II. As in figure 2, solid lines are only for eye guidance.

3. Composition fluctuation in non-phase separating binary mixtures

Composition fluctuations in binary mixtures play important role both in equilibrium and dynamic behaviour[37–40]. The study of composition fluctuation may also provide useful information in understanding the origin of the strong non-ideal behaviour in the composition dependence of binary mixtures[23]. In this section, we present molecular dynamics simulation analysis of composition fluctuation in model I, which has been described in last section. In this model, both the species (A and B) have the same mass and diameter but different inter-molecular interactions, which are modelled by the Lennard–Jones potential. The interaction parameters are: $\epsilon_{AA} = 1{\cdot}0$, $\epsilon_{BB} = 0{\cdot}5$,

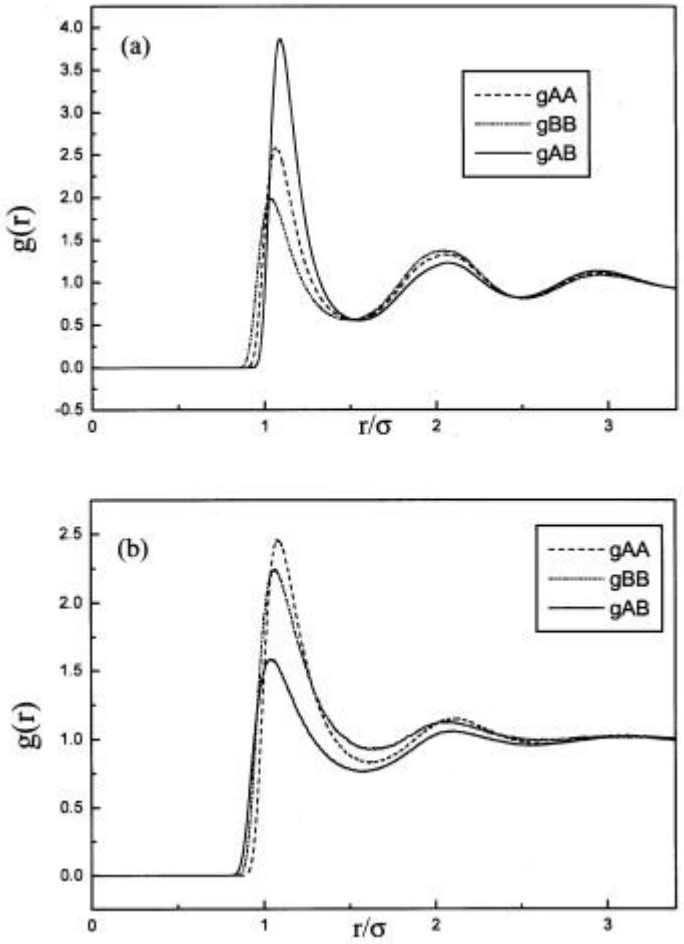

Figure 4. Radial distribution function for models I and II. All the partial radial distribution functions g_{AA} (solvent–solvent), g_{AB} (solvent–solute) and g_{BB} (solute–solute) are plotted for 0·4 solute composition; (**a**) shows the results for model I and (**b**) shows the same for model II. In both cases, dashed lines show g_{AA}, short dashed lines show g_{BB} and solid lines show g_{AB}.

$\epsilon_{AB} = 2.0$. We find that the composition fluctuation is nearly Gaussian for both the species, the width and the height of the peak being determined by the composition.

3.1 *Simulation details*

The simulations methodology remains nearly the same as that described in the previous section (for the micro-canonical NVE ensemble) except for the calculation of the composition fluctuations[40]. The calculation of composition fluctuation has been incorporated into the simulation in the following manner. Nine hypothetical spheres of radius 2σ have been incorporated into the simulation box. After the equilibration (which is carried out in the usual manner as mentioned in the previous section), at each

time step the total number of both the components (A and B) present in each sphere is calculated separately. This has been done by calculating the distance of each particle from the centre of the sphere. After the execution of simulation, overall average of components A and B is determined by,

$$\langle N_{\mathrm{A}}^{\mathrm{R}} \rangle = \frac{1}{N_s} \sum_{i=1}^{N_s} \overline{N}_i^A, \tag{16}$$

where the summation is over the number of the spheres N_s, N_i^{A} representing the number of A particles in the ith sphere and $\overline{N}$ denoting time-averaging over a fixed sphere. ⟨B⟩ is determined in a similar way. Then, fluctuation in number $N_{\mathrm{A}}^{\mathrm{R}}$ in a fixed sphere of radius R is defined by,

$$\delta N_{\mathrm{A}}^{\mathrm{R}} = N_{\mathrm{A}}^{\mathrm{R}} - \langle N_{\mathrm{A}}^{\mathrm{R}} \rangle, \tag{17}$$

and similarly for species *B*.

3.2 *Probability distribution of composition fluctuation*

Figure 5 shows the normalized probability distributions of the composition fluctuation for both the components at $x_{\mathrm{B}} = 0{\cdot}6$ in the sphere of 2σ radius. Figure 5a shows the composition fluctuation of component A, while that of B is shown in figure 5b. In both the figures the simulation results are depicted by the histograms. The full line represents the Gaussian fit. As can be seen from these figures, the probability for the composition fluctuation is nearly Gaussian, centred around the average value of the respective components in both the cases. Nevertheless, on going from the minority species (A) to the majority species (B), not only does the peak height decreases but the peak also becomes broader (as can be seen from the figures 5a and b). This variation in fluctuation is expected. Similar results have been obtained at other compositions. In figure 5, the average number of components A and B are $\langle A \rangle = 11{\cdot}39$ and $\langle B \rangle = 17{\cdot}00$, respectively. Thus, the local number density fluctuation is rather large. This could be the reason for the non-ideality in viscosity. We recall that a large fluctuation in shear stress was also obtained from microscopic calculation, using (5). However, irrespective of the fluctuation in A and B, the average number of all the particles present in a sphere remains nearly constant (28·4) for all the compositions. Thus, even for a sphere of radius $R = 2\sigma$, total density fluctuation is small.

4. Re-entrant orientational relaxation in binary mixtures

Conventionally, the rotational diffusion (D_R) coefficient of a solute is given by the well-known Debye–Stokes–Einstein (DSE) relation,

$$D_R = \frac{k_B T}{8\pi\eta r_s}, \tag{18}$$

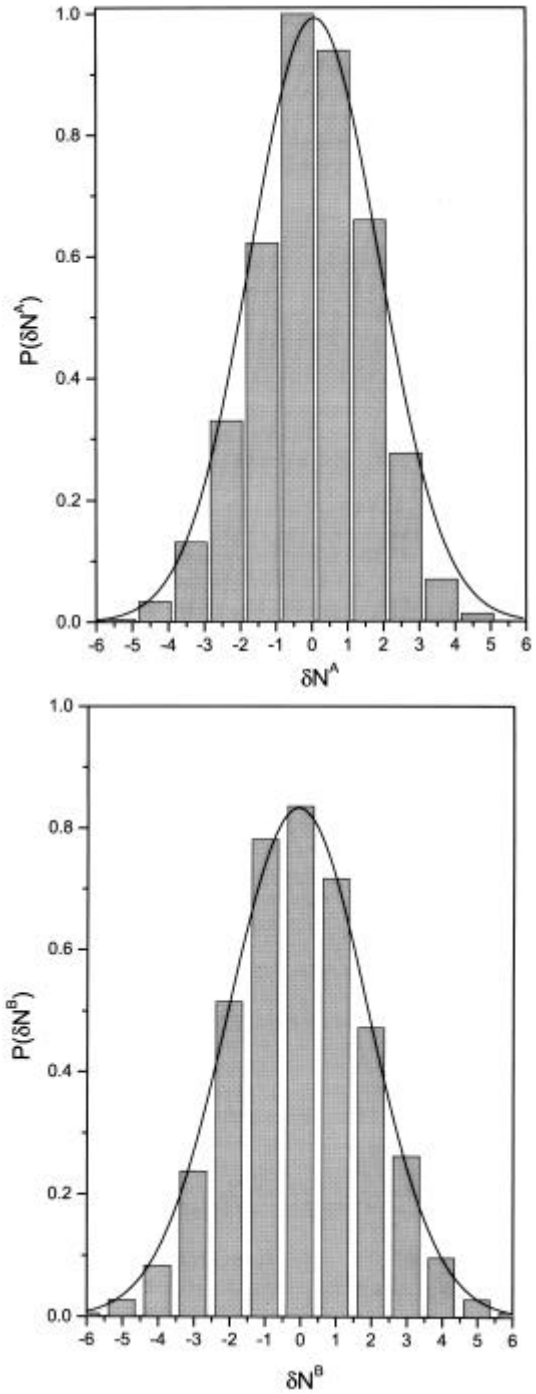

Figure 5. Normalized probability distribution of composition fluctuations in model-I binary mixtures at 0·6, B composition; (**a**) shows the composition fluctuation of A components within a sphere of radius 2 *s*; (**b**) shows the same for the B components. In both the figures, the histogram denotes simulation results and the full line represents the Gaussian fit.

where k_BT is the Boltzmann constant times the temperature (T), η is the viscosity of the liquid medium and r_s is the radius of the molecule. Experimentally, one measures the orientational time correlation function $C_\ell(t)$ (ℓ is the rank of the spherical harmonic coefficients), with $\ell = 1$ or 2. Now if the Debye rotational diffusion model is assumed, the relaxation time $\tau_{\ell R}$ is given by,

$$\tau_{\ell R} = [\ell(\ell+1)D_R]^{-1}, \tag{19}$$

where D_R is the rotational diffusion coefficient. Thus, according to the hydrodynamic theory the viscosity is a unique determinant of the rotational relaxation time. As discussed in the introduction, there exists a multiple time scale in a binary mixture. Given the diversity present in the system it is naive to expect a simple proportionality between $\tau_{\ell R}$ and η to hold.

The breakdown of the hydrodynamic theory was dramatically exhibited by Beddard *et al*[4]. They used the picosecond fluorescence depolarization technique to study the rotational relaxation time of the dye cresyl violet in ethanol–water mixture by varying the ethanol–water composition. They reported different rotational relaxation times in solutions at the same viscosity but different compositions.

This re-entrant type of behaviour of the orientational relaxation time when plotted against viscosity is yet to be explained. Although the viscosity itself in a binary mixture is known to exhibit non-ideal behaviour (as has been discussed in the previous section) it should be noted that the composition dependence of the orientational relaxation time cannot be understood only in terms of this non-ideality in viscosity. Re-entrance is strongly dependent on the specific interaction of the solute with the solvents as has already been discussed by Beddard *et al*[4]. The role of specific interaction in the orientational dynamics has often been discussed and the effect has been included in the DSE relation by changing the boundary condition[41,42]. However, to the best of our knowledge, a detailed study of the rotational dynamics in a binary mixture has not been carried out before.

Extensive MD simulations at constant pressure (P), temperature (T) and total number of molecules (N) have been carried out to study the orientational relaxation of prolate ellipsoids in several binary mixtures. We find that the orientational relaxation time of the ellipsoid when plotted against the solvent viscosity, does indeed show re-entrance.

4.1 *Systems and simulation details*

Here we present molecular dynamics NPT simulations of rotational correlation time τ_{2R} of tagged, isolated, Gay–Berne ellipsoids[43] in a binary mixture of Lennard–Jones spheres. The two species of the binary mixture are denoted by (A) and (B), as in the previous sections. The composition of the binary mixture is varied from 0 to 1, where composition '0' denotes all (A) particles and composition '1' denotes all (B) particles. The total number of molecules in the system is 504, where there are 4 ellipsoids which are placed far from each other and 500 solvents which includes both (A) and (B) types of molecules.

The interaction between the particles is modelled by different potentials. The interaction between the spheres in the binary mixture is given by the Lennard–Jones 12-6 potential,

$$U_{ij} = 4\varepsilon_{ij}\left[\left(\frac{\sigma}{r_{ij}}\right)^{12} - \left(\frac{\sigma}{r_{ij}}\right)^{6}\right], \tag{20}$$

where i and j denote two different particles which can be both (A) or both (B) or one (A) and the other (B).

Interaction energy between two ellipsoids with arbitrary orientations is assumed to be given by the Gay–Berne potential [43]

$$U_{GB} = 4\varepsilon(\hat{r}, \hat{u}_1, \hat{u}_1)\left[\left[\frac{1}{r - \sigma(\hat{r}, \hat{u}_1, \hat{u}_2) + 1}\right]^{12} - \left[\frac{1}{r - \sigma(\hat{r}, \hat{u}_1\hat{u}_2) + 1}\right]^{6}\right], \tag{21}$$

where $\hat{u}_1, \hat{u}_2$ are the axial vectors of the molecules 1 and 2 respectively. $\hat{r}$ is the vector along the intermolecular separation $r = r_2 - r_1$, where r_1 and r_2 denote the centres of mass of ellipsoids 1 and 2 respectively. $\sigma(\hat{r}, \hat{u}_1, \hat{u}_2)$ and $\varepsilon(\hat{r}, \hat{u}_1, \hat{u}_2)$ are the orientation-dependent range and strength parameters respectively. σ and ε depend on the aspect ratio κ which is the ratio between the semi-major and the semi-minor axes of the ellipsoids. Finally, the interaction between a sphere and an ellipsoid is accounted for by a modified GB–LJ potential as given below [43,45]

$$U_{Ei} = 4\varepsilon_{Ei}\left[\left[\frac{\sigma(\theta)_{Ei}}{r}\right]^{12} - \left[\frac{\sigma(\theta)_{Ei}}{r}\right]^{6}\right], \tag{22}$$

where E denotes the ellipsoids and i can be either (A) or (B).

$$\sigma(\theta)_{Ei} = \frac{(b/2 + R_i)}{(1 - X^2\cos^2\theta)^{1/2}}, \tag{23}$$

where θ is the angle between the major axis of the ellipsoid and the vector joining the centres of the sphere and the ellipsoid.

$$R_i = \sigma_i / 2, \tag{24}$$

$$X = \left(\frac{\bar{a}^2 - b^2/4}{\bar{a}^2 + R_i^2}\right)^{1/2}, \tag{25}$$

and

$$\bar{a} = \left((b^2 + R_i^2)\left(\frac{L/2 + R_i}{b/2 + R_i}\right)^2 - R_i^2\right)^{1/2}, \tag{26}$$

L is the major axis of the ellipsoid and b is the minor axis of the ellipsoid.

All the quantities in the simulation were scaled to appropriate units. The density by σ_{BB}^{-3} the temperature by ε_{AA}/k_B and the time by $(m_B\sigma_B^2/\varepsilon_{AA})^{1/2}$ – the scaled quantities are denoted by r^*, T^* and t^* respectively.

All the simulations have been carried out at $P = 1{\cdot}0$ and $T = 1{\cdot}0$. The system parameters corresponding to the interaction are, $\varepsilon_{BB} = 0{\cdot}7$, $\varepsilon_{AA} = 1{\cdot}0$, $\varepsilon_{AB} = 1{\cdot}5$, $\varepsilon_{EB} = 1{\cdot}4$ and $\varepsilon_{EA} = 0{\cdot}3$, while that of the masses are, $m_A = 0{\cdot}33$, $m_B = 1{\cdot}0$, $m_E = 1{\cdot}0$, and the distances are $\sigma_B = 1{\cdot}0$, $\sigma_A = 0{\cdot}66$, $a = 10$ and $L = 2{\cdot}0$.

The time step Δt used in the simulation is 0.0005 (t^*). The system was equilibrated for $1{\cdot}5 \times 10^5$ time steps and after that the averages were obtained for another 2×10^5 time steps. In each case we have executed at least *five* independent simulations and results presented are the averages over all the five different simulation runs.

4.2 *Results and discussions*

Figure 6 shows the re-entrant behaviour. Here the rotational relaxation time is plotted against the viscosity by varying the composition. The maximum of the viscosity is obtained at composition 0·4 where its value is 2·66 times the value at $c_B = 0$. The rotational relaxation time varies by a factor of 1·5. The essence of re-entrance is nicely captured in figure 6.

Note that although figure 6 has the same qualitative features as the experimental plot [4], there exist some differences in the intrinsic details. The details of the plot can be easily alerted by tuning the interactions.

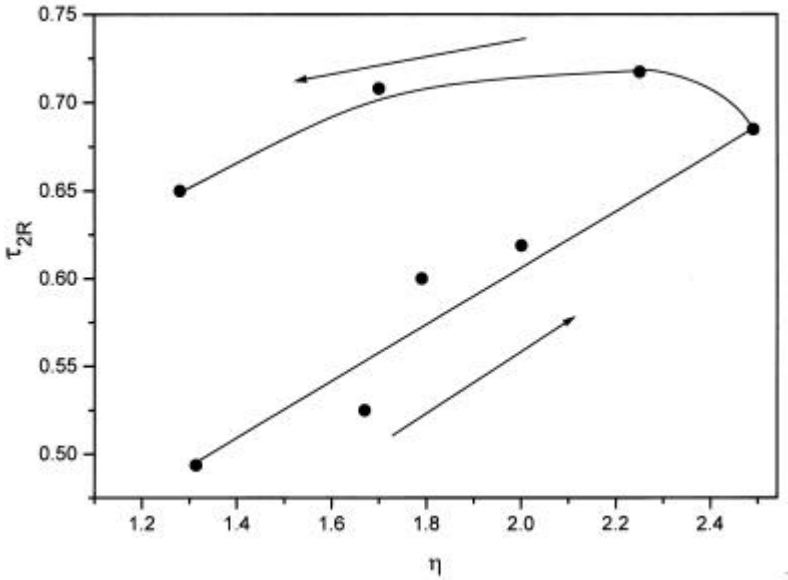

Figure 6. Reduced orientational relaxation time, t_{2R}, plotted against the reduced viscosity of the binary mixture, h, is shown by the filled circles. t_{2R} shows a re-entrance. The solid line is a guide to the eye. The compositions of the solvent (B) are 0·04, 0·08, 0·15, 0·2, 0·4, 0·6, 0·8, and 1·0, where the direction of the arrows shows the increasing composition of (B) particles. The study is performed at $T^* = 1{\cdot}0$ and $P^* = 1{\cdot}0$.

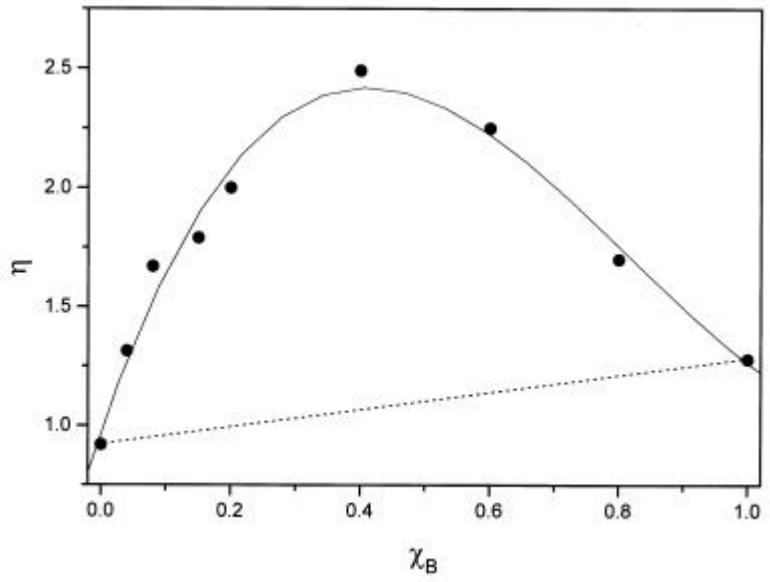

Figure 7. Composition dependence of the reduced viscosity is shown by the filled circles. The solid line is a guide to the eye. The dashed line shows the ideal behaviour of viscosity in a binary mixture. The study is performed at $T^* = 1{\cdot}0$ and $P^* = 1{\cdot}0$.

In figure 7 we have plotted the viscosity against the composition. The viscosity shows non-ideal behaviour. Ideal behaviour is given by the dotted line. The plot clearly shows that the viscosity in the binary mixture does show non-ideal behaviour and this has already been discussed at length in §2.

We next investigate whether the non-ideality in viscosity alone can reproduce the observed re-entrance in orientational relaxation time. In figure 8 we have shown the ratio of $\tau_{2R}(c)/\tau_{2R}$ $(c = 0{\cdot}04)$ against the ratio $\eta(c)/\eta$ $(c = 0{\cdot}04)$. The dashed line is the result obtained from the DSE relation where τ_{2R} is calculated from (18) and (19), by using the viscosities plotted in figure 7. From the figures, it is obvious that *the non-ideality in viscosity in a binary mixture alone cannot explain the re-entrance.*

The study here shows that in a system where the solute interacts differently with the two different species in a binary mixture, its rotational relaxation depends more on the composition than on the viscosity of the binary mixture. Thus, re-entrant type behaviour is strongly dependent on the interactions of the solute with the two different species making up the solvent.

5. Heterogeneous dynamics in supercooled liquid

Recent experiments, simulations and theoretical studies all seem to suggest the presence of heterogeneous dynamics in a supercooled liquid[46]. This heterogeneity in the kinetics is believed to have originated from the free energy landscape with multiple minima and maxima[11,47]. Although many characteristics of the free energy functional have been qualitatively calculated from the q-spin Potts model[48], the connection between the dynamics and the free energy landscape is not fully clear. Even the nature of the heterogeneity (entropic or density) is not understood yet.

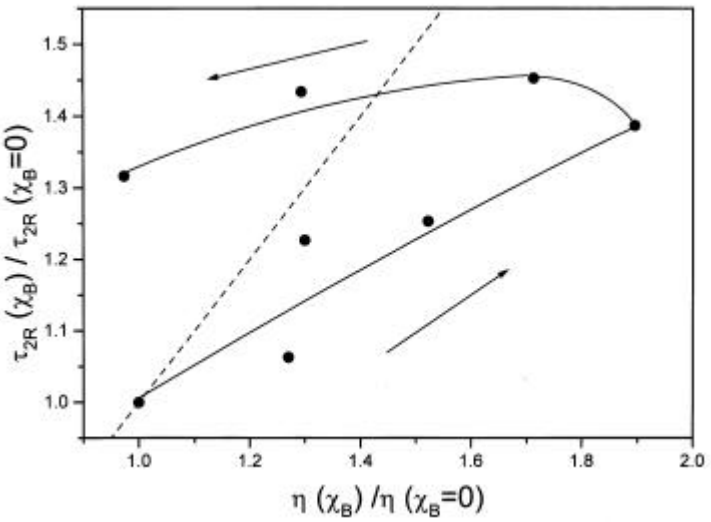

Figure 8. The ratio $t_{2R}(c_B)/t_{2R}(c_B = 0)$ against the ratio $h(c_B)/h(c_B = 0)$ is shown by the filled circles. The solid line is an aid to the eye. The dashed line shows the plot of the same but here $\tau_{2R}(c_B)$ is calculated from (18) and (19) of the text using the simulated viscosities. The compositions of the solvent are the same as in figure 6 and the directions of the arrows show the increasing composition of (B) particles. The study is performed at $T^* = 1{\cdot}0$ and $P^* = 1{\cdot}0$.

The most direct experimental evidence of the heterogeneous relaxation comes from NMR and fluorescence depolarisation studies of the tagged probes in supercooled liquids [46]. These experiments measure translational and orientational relaxation of the probe molecules. The advantages of using the orientational relaxation as a probe of heterogeneity are many-fold. First, the orientational relaxation is mostly a local phenomenon and thus explores only the local dynamics. Second, the orientational relaxation is faster than the density relaxation, therefore the density relaxation and orientational dynamics are well-separated in time.

We are not aware of any theoretical or computer simulation study of heterogeneity by using solute orientational relaxation as the probe. Here we present an NPT–MD simulation study of the orientational relaxation of a tagged solute in a model, supercooled, binary mixture. The study shows the presence of widely different orientational dynamics of solutes at different locations in the same solvent.

5.1 *Simulation details*

Details of simulation are nearly the same as described in the foregoing sections. The simulations have been carried out at constant pressure (P), temperature (T), and constant total number of particles (N). In the binary mixture let us denote the two species as A and B. The total number of molecules in the system are 504, of which there are 4 ellipsoids which are placed far from each other and 400 of type A and 100 of type B solvents.

The potentials used in the simulations are the same as presented in the previous section, (20)–(26)). The parameters in the binary mixture are chosen such that it

represents the Kob–Andersen model[8,9], that is, $\epsilon_{AA} = 1{\cdot}0$, $\epsilon_{BB} = 0{\cdot}5$, $\epsilon_{AB} = 1{\cdot}5$, and $\sigma_A = 1{\cdot}0$, $\sigma_B = 0{\cdot}88$, $\sigma_{AB} = 0{\cdot}8$. The ellipsoid–sphere interactions are given by: $\epsilon_{EB} = 1{\cdot}0$, $\epsilon_{EA} = 1{\cdot}0$. The masses of the spheres and ellipsoids are all the same. The minor and major axes of the ellipsoid are given by $b = 1{\cdot}0$, and $L = 2{\cdot}0$. All the simulations reported here have been carried out at $P = 10{\cdot}0$ and $T = 0{\cdot}8$. The time step Δt used to simulate is 0·002. The system was equilibrated for $1{\cdot}5 \times 10^5$ time steps, after which the averages were obtained over another 3×10^6 time steps.

5.2 *Results and discussions*

In figure 9 we plot the orientational time correlation function of the 4 tagged ellipsoids located at different regions. The figure clearly shows the presence of heterogeneous dynamics in the supercooled liquid as probed by the orientational dynamics of the ellipsoids. The initial decay of the orientational time correlation function of all the 4 ellipsoids (till $C_{2R}(t) = 0{\cdot}9$), due to their inertial motion, are similar. However, after this initial decay, the orientational time correlation functions of all the ellipsoids behave differently. OCF of ellipsoid 1 and 4 decays with nearly the same time scale but that of particle 2 decays with a slightly longer time scale. On the other hand, the orientational time correlation function of ellipsoid 3 seems to saturate after decaying to 0·7. This implies the existence of 3 different dynamic regions even within such a small system.

In order to further investigate the nature of these regions, we have calculated two particle radial distribution functions, individually, for all the four ellipsoids. These are shown in figures 10a and b. The radial distribution functions show that ellipsoid 3 has

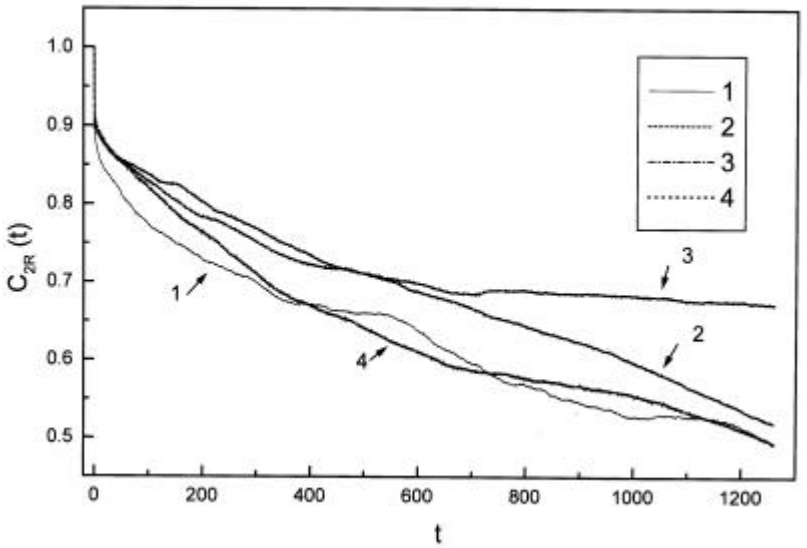

Figure 9. The orientational correlation function, $C_{2R}(t)$, is plotted against reduced time, individually, for 4 ellipsoids. The plot shows the presence of heterogeneous dynamics present in the binary mixture, as probed by the orientational dynamics of the ellipsoids. The solid line is for ellipsoid 1, the dashed line is for ellipsoid 2, the dashed-dot line is for ellipsoid 3 and the dotted line is for ellipsoid 4. The study is performed at $T^* = 0{\cdot}8$ and $P^* = 10{\cdot}0$.

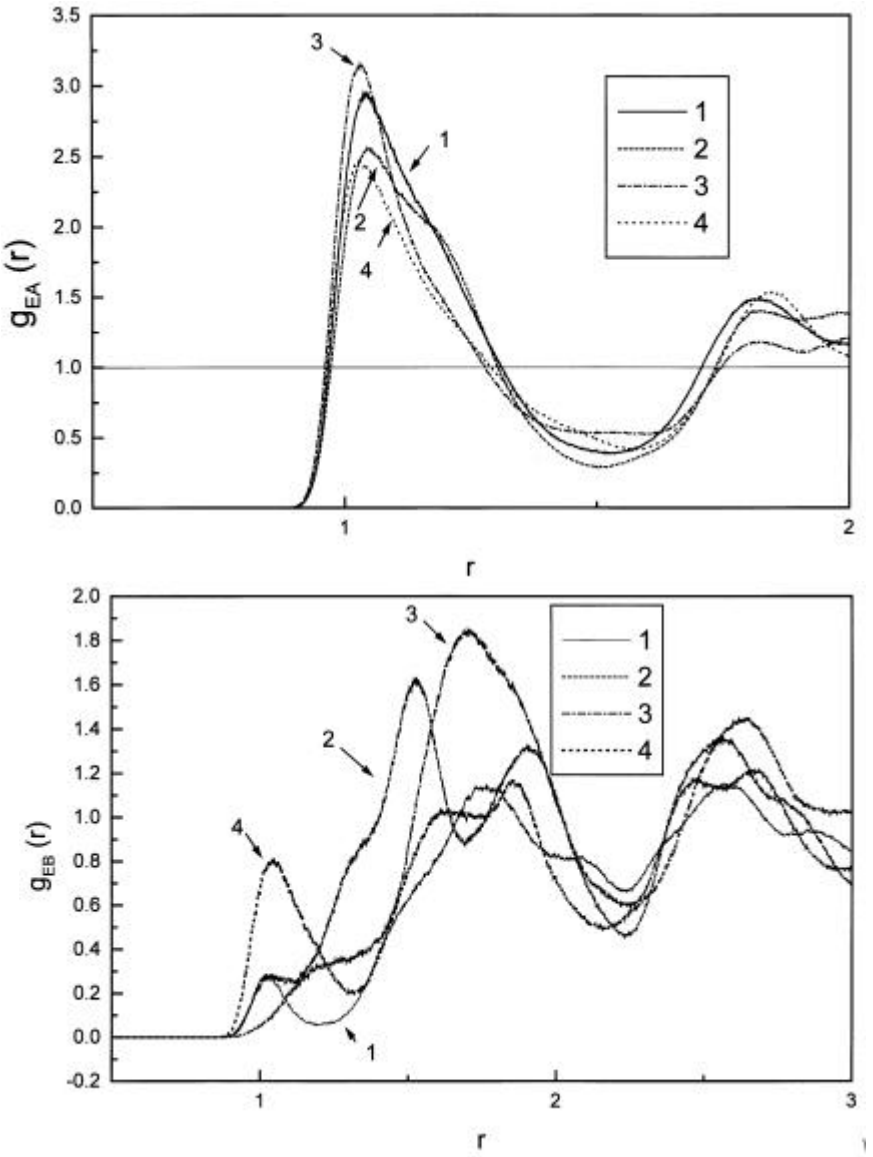

Figure 10. Radial distribution functions for the 4 ellipsoids; (**a**) shows the partial radial distribution function g_{EA} (ellipsoid–solvent A). The solid line is for ellipsoid 1, the dashed line is for ellipsoid 2, the dashed-dot line is for ellipsoid 3 and the dotted line is for ellipsoid 4; (**b**) shows the partial radial distribution function g_{EB} (ellipsoid–solvent B). Lines denote ellipsoids 1–4 as in figure (a).

the maximum number of neighbouring A particles. The B particles surrounding ellipsoid 3 are mostly at a distance, $r = 1{\cdot}5s$. Thus, the B particles are positioned mostly at the tip of the ellipsoid 3. Since the B particle is smaller than the ellipsoid, its dynamics takes place at a smaller time scale. On the other hand, the dynamics of the larger A particle is much slower than the rotational dynamics of the ellipsoid. As the

rotation of the ellipsoid is facilitated when there are more mobile particles on its sides rather than at the tips, the presence of more A particles around ellipsoid 3 hinders its rotational motion.

Thus we can argue that at the pressure and temperature we have studied and within 1·2 ns timeframe, A particle motion is almost frozen while B particles are mobile. This is similar to the prediction of Bosse *et al*[49] who performed a mode coupling theoretical calculation of binary mixtures of disparate size and have shown that although the larger particles form a glass, the smaller particles remain mobile.

The picture might be different for different probes. If the solute is large and massive then its timescale of rotation will be large and thus it will probe a more homogeneous solvent dynamics. To observe heterogeneity, the time scale of the rotational dynamics should be in-between the time scale of the dynamics of A and B.

6. Conclusions

In this article we have addressed several aspects of the dynamics of binary mixtures, which show exotic behaviour, that have eluded microscopic explanation. We show here that by proper modelling and tuning of the interaction parameters, many of these properties can be determined from theoretical and simulation studies.

Binary mixtures continue to be an area of active research. Although much of the recent interest is focused on the ability to model relaxation in supercooled liquids (as binary mixtures are good glass formers), we show here that study of composition dependence may help in understanding many aspects of the dynamics of binary mixtures and may even help in understanding dynamic properties of supercooled liquids.

The models presented here can be extended in several ways. We are currently investigating the relaxation dynamics of a mixture of spheres and ellipsoids. This system should retain the diversity of binary mixtures experienced here and in addition, incorporate the richness of orientational dynamics. We are also investigating the pressure dependence of viscosity and diffusion coefficients. At low to intermediate pressures, we find exponential pressure dependence of viscosity and the diffusion coefficient. We hope to address these problems in future.

Acknowledgements

It is a pleasure to thank Dr Srikanth Sastry for many useful discussions, both about NPT simulations and binary mixtures. This work was supported in part by grants from the Department of Science and Technology (DST), and the Council of Scientific and Industrial Research (CSIR), India. GS thanks the CSIR for a fellowship.

References

1. Kirkwood J G and Buff F P 1951 *J. Chem. Phys.* **19** 774
2. Qunfang L and Yu-Chun H 1999 *Fluid Phase Equilibria* **154** 153, and references therein
3. Pal A and Daas G 2000 *J. Mol. Liq.* **84** 327
4. Beddard G S, Doust T and Hudales J 1981 *Nature* (*London*) **294** 145
5. Chandra A and Bagchi B 1991 *J. Chem. Phys.* **94** 8367
6. Bagchi B and Chandra A 1992 *J. Chem. Phys.* **97** 5126
7. Bagchi B and Chandra A 1991 *Adv. Chem. Phys.* **80** 1

8. Kob W and Andersen H C 1995 *Phys. Rev.* **E51** 4626
9. Kob W and Andersen H C 1994 *Phys. Rev. Lett.* **73** 1376
10. Sastry S, Debenedetti P G and Stillinger F H 1998 *Nature* (*Lodnon*) **393** 554; Sastry S 2000 *Phys. Rev. Lett.* **85** 590
11. Sastry S 2001 *Nature* (*London*) **409** 164
12. Bhattacharyya S and Bagchi B 2001 *J. Phys. Chem.* **115** (in press)
13. Bhattacharyya S, Mukherjee A and Bagchi B 2001 *Phys Rev. Lett.*
14. Berry R S, Rice S A and Ross J 2000 *Physical chemistry* (New York: Oxford University Press)
15. Zwanzig R 1965 *Annu. Rev. Phys. Chem.* **16** 67
16. Zwanzig R and Mountain R D 1965 *J. Chem. Phys.* **43** 4464
17. Bagchi B and Bhattacharyya S 2001 *Adv. Chem. Phys.* **116** 67
18. Balucani U and Zoppi M 1994 *Dynamics of liquid state* (Oxford: Clarendon)
19. Sjogren L and Sjolandar A 1979 *J. Phys.* **C12** 4369
20. Bhattacharyya S 1999 Ph D thesis, Indian Institute of Science, Bangalore
21. Balucani U, Vellauri R and Gaskell T 1988 *Phys. Rev.* **A37** 3386
22. Bhattacharyya S and Bagchi B 1998 *J. Chem. Phys.* **109** 7885
23. Srinivas G, Mukherjee A and Bagchi B 2001 *J. Chem. Phys.* **114** 6220
24. Bosse J, Gotze W and Lucke M 1978 *Phys. Rev.* **A17** 434
25. Geszti T 1983 *J. Phys.* **C16** 5805
26. Madden W G and Rice S A 1980 *J. Chem. Phys.* **72** 4208
27. Chandra A and Bagchi B 2000 *J. Chem. Phys.* **112** 1876
28. Mukherjee A, Srinivas G and Bagchi B 2001 *Phys. Rev. Lett.* **86** 5926
29. Mukherjee A and Bagchi B 2001 *J. Phys. Chem.* (submitted)
30. Stoddard S D and Ford J 1973 *Phys. Rev.* **A8** 1504
31. Heyes D M 1988 *J. Chem. Phys.* **37** 5677
32. Andersen H C *et al* 1984 *Rapport d'activite scientifique du CECAM,* pp 82–115 [7.4, 7.4.3]
33. Brown D and Clarke J H R 1984 *Mol. Phys.* **51** 1243
34. Srinivas G, Bhattacharyya S and Bagchi B 1999 *J. Chem. Phys.* **110** 4477
35. Biswas R, Bhattacharyya S and Bagchi B 1998 *J. Phys. Chem.* **B102** 3552
36. Lynden-Bell R M and Rasaiah J C 1997 *J. Chem. Phys.* **107** 1981
37. Pratt L R 1990 *J. Am. Chem. Soc.* **112** 5071
38. Pratt L R and Chandler D A 1977 *J. Chem. Phys.* **67** 3683
39. Takamuku T *et al* 2001 *J. Phys. Chem.* **B105** 6236
40. Murarka R K, Srinivas G and Bagchi B 2001 *J. Phys. Chem.* (submitted)
41. Montegomery J A and Berne B J 1977 *J. Chem. Phys.* **67** 4580
42. Lynden-Bell R M and Rasaiah J C 1997 *J. Chem. Phys.* **107** 1981
43. Gay J G and Berne B J 1981 *J. Chem. Phys.* **74** 3316
44. Ravichandran S and Bagchi B 1999 *J. Chem. Phys.* **111** 7505
45. The potential has been developed and tested in collaboration with Dr Perera A of LPTL, Univ. P. et M. Curie, Jussieu, Paris 75252 (private communication). This potential was used in Ref. 10 and shown to give consistent results
46. Ediger M D, Angell C A and Nagel S R 1996 *J. Phys. Chem.* **100** 13200; Cicerone M T and Ediger M D 1996 *J. Chem. Phys.* **104** 7210; Cicerone M T and Ediger M D 1996 *J. Chem. Phys.* **103** 5684; Cicerone M T, Blachburn F R and Ediger M D 1995 *J. Chem. Phys.* **102** 471; Cicerone M T, Blachburn F R and Ediger M D 1995 *Macromolecules* **28** 8224; Heuberger G and Sillescu H 1996 *J. Chem. Phys.* **100** 15255
47. Wolynes P G 1997 *Proc. Natl. Acad. Sci. USA* **94** 11037; Brooks III C L, Martin Gruebele, Onuchic J N and Wolynes P G 1998 *Proc. Natl. Acad. Sci. USA* **95** 11037
48. Kirkpatrick T R, Thirumalai D and Wolynes P G 1989 *Phys. Rev.* **A40** 1045
49. Bosse J and Kaneko Y 1995 *Phys. Rev. Lett.* **74** 4023